Slant Visual Range Calculated by Use of SCOTRAN Contrast Transmittance Model

G. H. Ruppersberg, R. H. Buell, R. Schellhase

DFVLR, Institut für Physik der Atmosphäre, 8031 Weßling/Obb.

Abstract:

The SCOTRAN contrast transmittance model is at the heart of a slant visual range model. It solves the equation of transfer for the special case of visual range in a reasonable computing time with the aid of model formulations, and reduces the contrast transmittance in the atmosphere to observational and environmental parameters which can be measured or given in practice. The slant visual range model processes these values, together with the target parameters and contrast threshold functions applicable in the individual case, to give the slant visual range. The slant visual range V_{CS} of large, (subtending more than 20 minutes of arc = 5.8 mrad) black and not self-luminous targets can, however, already be supplied by SCOTRAN.

The model thus provides a clear and realistic overview of the influence of the various different observational and environmental parameters and also some target parameters on the slant visual range. The results are consistent with practical experience. They also have effects in some important practical situations which one would not have expected but which can be explained logically.

Zusammenfassung: Schrägsichtweite berechnet mit Hilfe des SCOTRAN Kontrast-Transmissions-Modells

Das Kontrasttransmissionsmodell SCOTRAN ist der Kern eines Schrägsichtmodells. Es löst die Strahlungs-übertragungsgleichung für den Spezialfall der Sichtweite mit Hilfe von Modellansätzen in angemessener Rechenzeit und führt den Kontrasttransmissionsgrad in der Atmosphäre auf Beobachtungs- und Umgebungs-parameter zurück, die man in der Praxis messen oder vorgeben kann. Das Schrägsichtmodell verarbeitet diese Werte in Verbindung mit den Objektparametern und Kontrastschwellenwertfunktionen, die für den Einzel-fall zutreffen, zur Schrägsichtweite. Die Schrägsichtweite V_{CS} von großen (mehr als 20 Bogenminuten = 5,8 mrad aufspannenden), schwarzen und nicht selbstleuchtenden Objekten kann aber schon von SCOTRAN aus-gegeben werden. Das Modell liefert damit eine deutliche und realistische Übersicht über den Einfluß der unterschiedlichen Beobachtungs-, Umgebungs- und auch einiger Objektparameter auf die Schrägsichtweite. Die Ergebnisse sind im Einklang mit der Erfahrung. Sie zeigen in praktisch wichtigen Situationen aber auch Effekte, die man nicht erwartet hätte, die sich jedoch widerspruchsfrei erklären lassen.

Résumé: Portée visuelle oblique calculée à l'aide d'un modèle SCOTRAN

Le modèle SCOTRAN de transmittance de contraste constitue l'essentiel d'un modèle de portée visuelle oblique. Il résout l'équation de transfert pour le cas spécial de la portée visuelle en un temps de calcul raisonnable et ramène la transmittance de contraste dans l'atmosphère à des paramètres d'observation et d'environnement qui peuvent être mesurés ou donnés dans la pratique. Le modèle de portée visuelle traite ces valeurs, en liaison avec les paramètres de la cible et les fonctions de seuil de contraste applicables dans le cas individuel, pour fournir la portée visuelle oblique. Cependant, la portée visuelle oblique V_{CS} d'objets grands (sous-tendant plus de 20 minutes d'arc = 5,8 mrad), noirs et non lumineux par eux-mêmes, peut déjà être donnée par SCOTRAN. Le modèle fournit donc une vue d'ensemble claire et réaliste de l'influence de divers paramètres d'observation et d'environnement, et aussi de paramètres de la cible, sur la portée visuelle oblique. Les résultats concordent avec l'expérience. Ils révèlent aussi, dans certaines situations pratiques importantes, des effets qu'on n'aurait pas attendus et qui peuvent être expliqués logiquement.

Beitr. Phys. Atmosph. Vol. 58, No. 1, February 1985

53

Symbols and Designations

Symbols and designations complying with CIE and DIN 5037 have been used as far as possible. As regards the extinction coefficient and related values we have followed the recommendations of KASTEN and RASCHKE (1972) and RASCHKE (1978). In accordance with DUNTLEY, JOHNSON and GORDON (1978) we have used indices on the left as "identifiers", in order to assign radiation quantities to certain objects or fields. We have deviated from the designations used by these authors only when the standards mentioned above make this appear advisable. Like DUNTLEY et al. we have not included the wavelength in the argument every time; nearly all the values are a function of the wavelength. The individual values are explained in the text.

1   Introduction

More than half a century ago KOSCHMIEDER (1925) published his theory of horizontal visual range in this journal. It is internationally recognized today and is also the basis of every type of visual range measurement. FOITZIKs (1947), DUNTLEYs (1948), and SIEDENTOPFs (1948) first works on a slant visual range are nearly 40 years old; they are the starting point for all attempts at solving the problem of slant visual range. But a description of the phenomenon, which although simple covers the essential, like KOSCHMIEDERs theory of horizontal visual range, is not successful for slant visual range. Modern computer technology, together with the impulses generated by the project OPAQUE (Optical Atmospheric Quantities in Europe; BAKKER, 1975; FENN, 1978; JOHNSON & GORDON, 1982) led, however, to new models for slant visual range. These offer for the first time a comprehensive overview of the interaction of the various observational, environmental and target parameters relating to slant visual range. This paper reports on these, dealing in particular with the contrast transmittance model SCOTRAN.

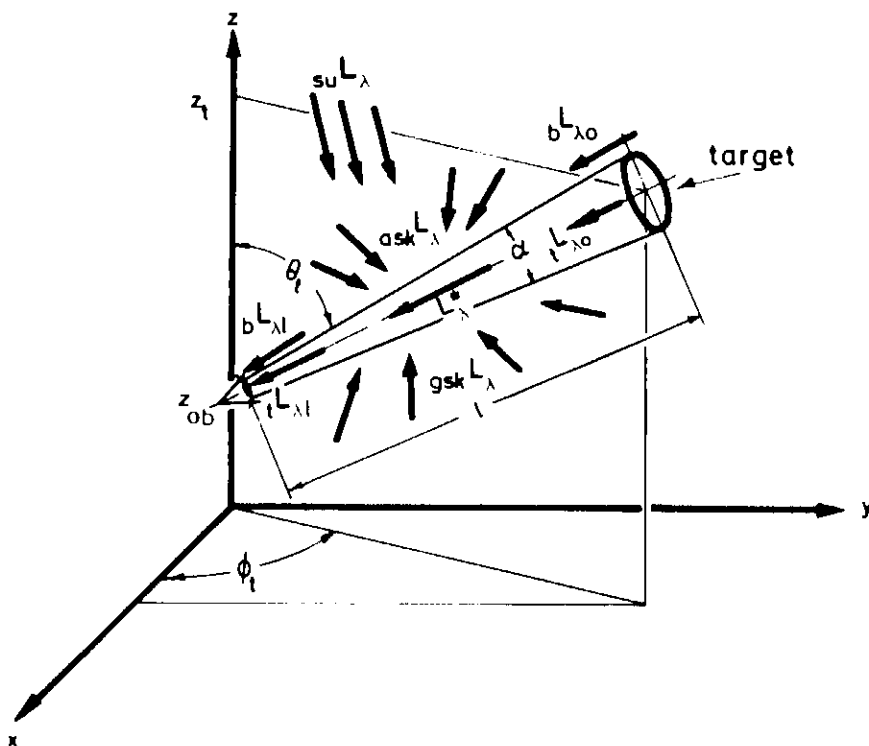## 2   From the Theory of Slant Visual Range to the Model

The visual range V (defined in accordance with HÖHN, 1981) is the horizontal component of the maximum distance between observer and target, up to which a particular viewing problem (e.g. detection, recognition, identification) can be solved under particular environmental conditions by a normal observer using a particular viewing device with a particular probability (50 % or "practically 100 %").

Specification of the horizontal component as the visual range V, rather than the maximum distance itself, complies with military aviation practice (WEISS, 1976). The difference is only significant when V is not large compared with the difference in height Δz between observer and target; e.g. for $V > 5 \times \Delta z$ it is less than 2 %.

A normal observer can resolve the given visual problem under given environmental conditions with a given viewing device with given probability if the apparent contrast

$$C_l(z_{ob}, \theta_t, \Phi_t) = \frac{{}_tL_{\lambda l}(z_{ob}, \theta_t, \Phi_t) - {}_bL_{\lambda l}(z_{ob}, \theta_t, \Phi_t)}{{}_bL_{\lambda l}(z_{ob}, \theta_t, \Phi_t)} , \tag{1}$$

with which the target appears to the observer or the viewing device is greater than the contrast threshold C' applicable for these conditions. ${}_tL_{\lambda l}$ and ${}_bL_{\lambda l}$ are the apparent spectral radiances of the target and the background, respectively, at the distance l between target and observer in the observation level z_{ob} and into the viewing direction θ_t, Φ_t (cf. Figure 1). These spectral radiances differ from the inherent spectral radiances ${}_tL_{\lambda o}$ and ${}_bL_{\lambda o}$ close to the target because the irradiated atmosphere on one hand attenuates the radiant fluxes between target and observer, and on the other hand adds its own path radiance L_λ^*

which is discussed later (cf. Equations (10) and (11). Thus apparent contrast generally differs from the inherent contrast

$$C_o(z_t, \theta_t, \Phi_t) = \frac{_tL_{\lambda o}(z_t, \theta_t, \Phi_t) - _bL_{\lambda o}(z_t, \theta_t, \Phi_t)}{_bL_{\lambda o}(z_t, \theta_t, \Phi_t)},$$

(2)

with which the target appears at close quarters. The contrast transmittance τ_c is given as a measure of this difference:

$$\tau_C(z_t, z_{ob}, \theta_t, \Phi_t) = \frac{C_l}{C_o}.$$

(3)

With these definitions the problem of visual range V can be expressed in the formula:

$$C_o\tau_C(|l_V \sin\theta_t| = V; \Phi_t) = C',$$

(4)

with

$$l_V = \frac{(z_t - z_{ob})_V}{\cos\theta_t}.$$

(5)

In other words the visual range V is the horizontal component of the distance l_V between target and observer at which (under the given environmental conditions) the product of inherent contrast C_o and contrast transmittance τ_c is equal to the threshold of contrast C' of the observer under the given conditions.

DUNTLEYs theory of slant visual range (cf. DUNTLEY, BOILEAU and PREISENDORFER, 1957) gives the following formula for contrast transmittance, disregarding only the shading of the path radiance in front of the target by the target itself, otherwise exactly:

$$\tau_C(z_t, z_{ob}, \theta_t, \Phi_t) = \frac{1}{1 + \dfrac{L_\lambda^*(z_t, z_{ob}, \theta_t, \Phi_t)}{\tau_r(z_t, z_{ob}, \theta_t) \, _bL_{\lambda o}(z_t, \theta_t, \Phi_t)}}.$$

(6)

Beitr. Phys. Atmosph. Vol. 58, No. 1, February 1985

55

As mentioned above, $_b L_{\lambda o}$ is the inherent spectral radiance of the background in the direction towards the observer, and the spectral path radiance L_λ^* is discussed in connection with Equations (10) and (11). The regular transmittance τ_r results from the vertical profile of the extinction coefficient $\sigma_e(z)$:

$$\tau_r(z_t, z_{ob}, \theta_t) = e^{- \operatorname{cosec} \theta_t \int_{z_t}^{z_{ob}} \sigma_e(z)\,dz} \ . \tag{7}$$

Horizontal homogeneity (but not isotropy) is assumed here — as it also clearly is in the argument of the other values. The influence of broken cloud on the path radiance can according to OVERINGTON (1976, Chapter 15.4) or JOHNSON and GORDON (1983, Chapter 3.2) be taken adequately into account by spatial averaging.

Contrast and visual range, however, differ considerably when the target is seen against a cloud and against a clear sky. The same also applies to air-ground observations when, for example, dark woodland is predominant in the field of vision and determines the path radiance of the background, while the target is searched for in a bright clearing. Both cases can be included simply:

Let $_b L_{\lambda o}$ in Equation (6) be the mean spectral inherent radiance (determining the path radiance) of the more distant target background, $_{tb} L_{\lambda o}$ be the spectral inherent radiance of the direct background, and let both differ by the factor k:

$$_{tb} L_{\lambda o} = k\ _b L_{\lambda o}. \tag{8}$$

It then follows from Equation (6) for the local contrast transmittance:

$$\tau_C^{(tb)} = \frac{1}{1 - (1 - 1/\tau_C)/k}\ . \tag{9}$$

τ_C is the contrast transmittance calculated by Equation (6).

Going back to Equation (6), the spectral path radiance L_λ^* is that spectral fraction of any radiation penetrating the viewing cone (cf. Figure 1) which is scattered towards the observer. It is useful to discriminate between the fractions caused by direct sun radiation and by the multidirectional hemispherical radiation, $_{su} L_\lambda^*$ and $_{sk} L_\lambda^*$ respectively:

$$L_\lambda^*(z_t, z_{ob}, \theta_t, \Phi_t) = {}_{su}L_\lambda^*(z_t, z_{ob}, \theta_t, \Phi_t) + {}_{sk}L_\lambda^*(z_t, z_{ob}, \theta_t, \Phi_t). \tag{10}$$

Assuming a standardized scattering function for the aerosol particles which is constant in each single layer, the first fraction, $_{su} L_\lambda^*$, can be reduced to the observational and environmental parameters by analytical integration. For the second fraction this equation applies:

$$_{sk}L_\lambda^*(z_t, z_{ob}, \theta_t, \Phi_t) =$$

$$= \int_{r \triangleq z_{ob}}^{z_t} \sigma_s(z)\,\tau_r(z, z_{ob}, \theta_t) \int_{\theta_{sk}=0}^{\pi} \int_{\Phi_{sk}=0}^{2\pi} \beta'(z, \varphi_{sk})\ _{sk}L_\lambda\,(z, \theta_{sk}, \Phi_{sk}) \sin\theta_{sk}\, d\theta_{sk}\, d\Phi_{sk}\, dr. \tag{11}$$

The hemispherical spectral radiances $_{sk}L_\lambda$ in the second integrand of Equation (11) are called $_{ask}L_\lambda$ for the upper and $_{gsk}L_\lambda$ for the lower hemisphere (cf. Figure 1). $_{ask}L_\lambda$ is nothing else than the path radiance from the space between the element of volume in question and the boundary of the atmosphere; $_{gsk}L_\lambda$ additionally includes the transmitted spectral radiance of the ground. Thus the one path radiance in the viewing cone to be found with Equation (11) cannot be calculated until the path radiances from the entire space affecting each element of the volume in the viewing cone have been determined.

This is a problem which cannot be solved analytically without making very restrictive assumptions. It can also be treated purely numerically with the most powerful large-scale computers — and purely experimentally only with considerable expenditure — only for a few sets of values for the observational, environmental and target parameters. None of these methods results in even only a rough overview of the whole subject of slant visual range:

DUNTLEY provided easy-to-follow analytical solutions early on with his two-constant theory of slant visual range (cf. also MIDDLETON, page 68 f. and page 122 f.). But he was obliged to introduce restrictive assumptions for this which prohibit some important applications. The contrast transmittance turns out, for example, to be independent of the azimuth in the viewing direction — which is not the case in some important practical situations — and the inherent contrast has to be given. In fact, however, the inherent contrast is the result of a complicated interaction of the observational, environmental and target parameters. In the case of ground-air vision, for example, the inherent contrast of an aircraft is a function not only of its flight position and the reflectance or the BRDF (bidirectional reflection distribution function) of the visible parts, but also of the sun's position, the sky background and the albedo of the space under it, which all have a lasting effect on the contrast transmittance as well.

If we restrict ourselves in the case of the numerical solution to the 13 observational, environmental and target parameters which are listed in Table 1, and allow just as many different values for each parameter as may be assumed to be necessary and adequate for detecting its influence on the slant visual range, then this gives 4.8×10^8 different sets of values. A computing time of only 1 s for solving each individual problem would result in a total computation time of 15 years — and the correct solution of Equation (11) even today still takes more than 1 s on the most powerful large computer. It is not possible to solve the problem purely experimentally either for the same reason.

In this case a slant visual range model can be of help:

Model notions are inserted in the numerical solution path which result in analytical solutions for individual stages demanding otherwise lengthy numerical calculations, thus drastically reducing total calculation time, but do not prevent a qualitatively correct and quantitatively usable reproduction of the curve of the slant visual range as a function of the observational, environmental and target parameters.

The calculated curve can be regarded as qualitatively correct if the trend is correct, i.e. for example if an actual decrease does not turn out as a constant value or even as an increase. Whether or not the result is usable in quantitative terms depends on the accuracy required in the intended application. In practice one is always forced to compromise on this for the simple reason that it is never possible to determine the state of the atmosphere exactly to the last detail, let alone predict it.

■ Table 1 Observational, environmental and target parameters, of which the slant visual range is a function. n individual values must probably be considered in order to detect the influence of this parameter on the slant visual range

No.	OBSERVATIONAL PARAMETERS	n	No.	ENVIRONMENTAL PARAMETERS	n	No.	TARGET PARAMETERS	n
1	wavelength	3	6	sun zenith distance	6	10	size and shape	3
2	height of target	16	7	turbidity stratification	8	11	orientation: azimuth	8
3	height of observer		8	cloudiness	4	12	orientation: zenith distance	3
4	azimuth ⎫ of	5	9	ground albedo or BRDF	6	13	BRDF	4
5	zenith ⎬ viewing	6						
	distance ⎭ direction							
	COMBINATIONS:	1440		COMBINATIONS:	1152		COMBINATIONS:	288

SLANT METEOROLOGICAL VISIBILITY: n = 8
CONTRAST TRANSMITTANCE MODEL: n = 1440*1152 = 1,659*10^6
SLANT VISIBILITY MODEL: n = 1440*1152*288 = 4,778*10^8

In the FASCAT contrast transmittance model HERING (1981) uses the algebraic approximation of HENYEY & GREENSTEIN (cf. HERING, 1981, p. 9 f.) for the normalized scattering function β', which turns up in the further development of $_{su}L_\lambda^*$ (Equation (10)), and the simpler delta EDDINGTON approximation (cf. HERING, 1981, p. 2) for the β' in Equation (11), because of the blurring caused anyway by multiple scattering. He replaces the hemispherical radiance $_{sk}L_\lambda$ in our Equation (11) by the sum of a first portion which is only z-dependent and another portion which is the product of another only z-dependent part and the cosine of the zenith angle. Equation (11) can thus be integrated analytically via θ_{sk} and Φ_{sk} and adequately simply by numerical means via r. The actual relationship between the azimuth and $_{sk}L_\lambda$ has, however, been suppressed with these approximations. The contrast transmittance τ_c (cf. Equation (6)) nevertheless proves to be a function of ϕ_t since the total path radiance L_λ^* is a function of the azimuth because of the direct sun radiation portion, and hence also the inherent radiance $_bL_{\lambda o}$ of the background.

Our SCOTRAN (= Slant Contrast Transmittance) model is described in the following section. It was developed at about the same time as FASCAT but independently (cf. v. REDWITZ et al., 1978; RUPPERS-BERG, 1979). In view of the physical notions described in the following chapter we come to a separation of the variables in Equation (11). This step is dictated almost inevitably by the problem itself; the steps followed by both models differ fundamentally before and after this operation. The comparison in Section 4 shows that the results of the two models agree remarkably well in certain areas, but differ from one another characteristically in others.

3   The SCOTRAN Contrast Transmittance Model

The SCOTRAN model developed at the DFVLR (cf. RUPPERSBERG, 1982; referred to as 'Ru' in the following) is a program system operating with optimized computing time, which solves the path radiance Equation (11) with the aid of parameterized relative radiance distributions, albedos and interpolation functions without physical contradictions and determines the contrast transmittance. The user enters a set of observational and environmental parameters which can be selected fairly freely (cf. Table 1). SCOTRAN then outputs the variation of the contrast transmittance due to the distance between target and observer, and the radiation field into which the target is placed.

A slant visual range model processes these values in conjunction with the target parameters and contrast threshold functions, e.g. of KASTEN (1962) or HOFFMANN (1983) applicable to the individual case to give the slant visual range. The contrast transmittance model is thus the heart of the slant visual range model. Its results can, however, also be illustrated with a special slant visual range (V_{CS}; cf. Section 4.2).

The internal structure of SCOTRAN is best understood with the help of Figure 2. The model starts out from a "two-plane-formulation". The two planes are at the reference altitudes z_m (e.g. at a height of 3000 m) and z_0 (e.g. at a height of 0 m). These delimit the upper and lower boundaries of the observation space.

In the observation space the turbidity stratification is entered as the vertical variation of the extinction ratio $Q_e(z)$, the extinction coefficient $\sigma_e(z)$ or, as in this paper, the meteorological visual range $V_N(z)$. At heights above z_m only the optical thickness $d(z_e, z_m)$ of the atmosphere above is of interest. The absorption factor σ_a/σ_e and the normalized scattering function $\beta'(\varphi)$ can change from a pregiven value or course to another in a "changeover level" z_s, e.g. at the top of a fog layer.

At both reference levels the model determines the relative radiance distributions $_{ask}\Lambda$ and $_{gsk}\Lambda$ of the upper and lower hemisphere which indicate how much greater or smaller the radiance of an area element is compared with the radiance of an isotropic hemisphere. At the lower reference level the relative radiance distribution of the lower hemisphere is $_{gsk}\Lambda^{(j)}(z_0) = \pi \times$ BRDF (= $\pi \times$ bidirectional reflection distribution function of the earth's surface; cf. Ru, Section 5.3.1); in the case of an isotropic surface it is equal to 1.
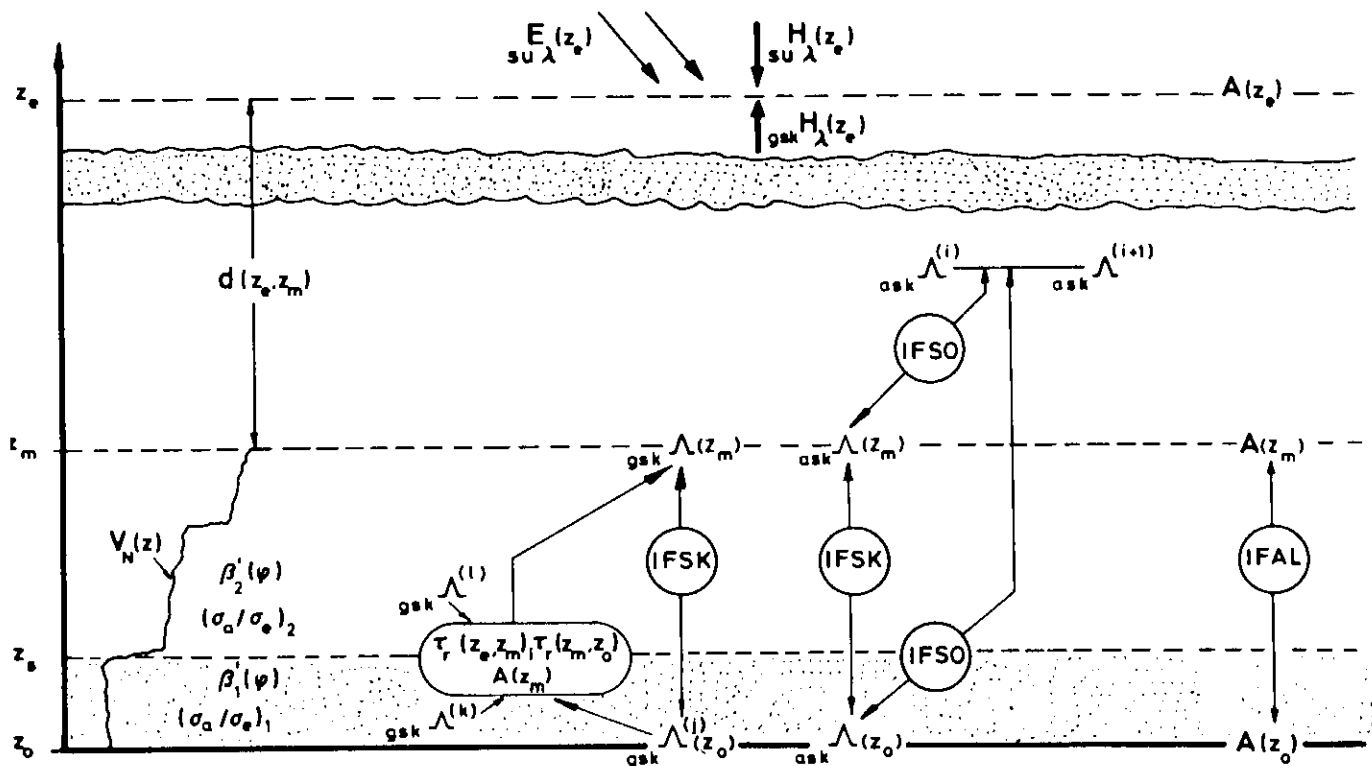
Figure 2 Inner structure of the SCOTRAN model. Description in the text.

At the upper reference level, z_m, this relative radiance distribution appears attenuated by the transmittance between the reference levels; to make up for this, different portions $_{gsk}\Lambda^{(l)}$ and $_{gsk}\Lambda^{(k)}$ from the single back-scattered sun radiation and the diffuse sky radiation are added up to $_{gsk}\Lambda(z_m)$ according to the transmittance for the directional sun radiation up to z_m and the albedo at this level.

For the relative radiance distributions of the upper hemisphere fixed distributions $_{ask}\Lambda^{(i)}$ are specified in the model for various sun zenith angles, ground albedos and optical thicknesses of the atmosphere above the level in question (Ru, Section 5.1.1 and 5.2.3).

The relative radiance distributions $_{ask}\Lambda(z_0)$ and $_{ask}\Lambda(z_m)$ are interpolated with an interpolation function IFSO between the distributions $_{ask}\Lambda^{(i+1)}$ and $_{ask}\Lambda^{(i)}$ which belong to the adjacent optical thicknesses. Between the reference levels the model interpolates the relative radiance distributions with the interpolation function IFSK.

One still needs the spectral vertical radiance flux densities of the diffuse hemisphere radiation, $_{sk}H_\lambda$ (Ru, Section 5.1.1), in order to arrive at the spectral radiances $_{sk}L_\lambda = (1/\pi)_{sk}\Lambda \ _{sk}H_\lambda$ of Equation (11). In SCOTRAN they are reduced to the albedos $A(z)$ (Ru, Section 5.3.2). In a process analogous to that described above for Λ, the model searches — at a given ground albedo $A(z_0)$ — for the reference value $A(z_m)$ and also $A(z_e)$ at the upper boundary of the atmosphere in the given tables of A for various sun zenith angles, ground albedos and optical thicknesses of the atmosphere above the reference level. Between the reference levels the model interpolates the albedo with the interpolation function IFAL.

The three interpolation functions IFSO, IFSK and IFAL are formulated as special functions of the optial thickness of the atmosphere involved. It is plausible to interpolate with functions of the optical thickness: If the radiance distributions or the albedo between the reference levels change significantly, if at all, this can only occur in optically thick layers, for example in ground fog, in a thin stratus layer or thick haze. The interpolation functions thus concentrate the changes in the range of increasing or decreasing optical thickness, where they with certainty actually take place.

IFSO controls the azimuth dependence of the calculated slant visual range between the curve forms which result at the given upper and lower optical thicknesses or degrees of cloudiness. Errors in IFSO therefore push the change of form too far into the range of the upper or lower optical thickness.

IFSK controls the azimuth dependence of the calculated visual range e.g. when the target or observer enters a layer of fog. Errors in IFSK cause the calculated dependence on azimuth angle to change too rapidly or too slowly on entering the fog layer.

IFAL controls the height dependence of the calculated slant visual range e.g. when the target or observer enters a layer of fog. Errors in IFAL cause too rapid or too slow changes of the calculated slant visual range in the z direction.

These model notions separate the variables z or r from the other independent variables in Equation (11). Moreover Λ takes the place of radiance $_{sk}L_\lambda$. The double integral need therefore only to be solved for the fixed values of $_{ask}\Lambda$ and $_{gsk}\Lambda$ in conjunction with the two different scattering functions β_1 and β_2 (cf. Figure 2) and tabulated as "INTA" and "INTG". Building on this only simple integrations are required (Ru, Section 5.4) which although requiring complicated program logic (BUELL, 1984) need only short calculation time.

At no point do the model notions contradict to energy conservation law. They satisfy the requirement mentioned earlier that the curve of the slant visual range as a function of the observational, environmental and target parameters is presented in a qualitatively correct and a quantitatively usable form. If desired the results can be improved in quantitative terms by providing refined parameterization for the fixed values of the relative radiance distributions and albedos and the interpolation functions.

The SCOTRAN version CIE 02 — whose results are discussed in Chapter 4 — like the earlier version CIE 01 (Ru) uses fixed values for the relative radiance distributions derived from CIE radiance distributions (Ru, Section 5.2.1), but the relative radiance distribution of the Sky Radiance Equation, in the Rayleight case (Section 3.1). The fixed values used for the albedo are the tables of PLASS and KATTAWAR (1968). An improved interpolation function IFAL (Section 3.2) is used for interpolation in CIE 02. The absorption component of the extinction coefficient is disregarded.

The CIE radiance distributions apply to the visual region of the spectrum and are here ascribed to the 550 nm wavelength. The results of the CIE model versions for this reason apply only to this wavelength, but may, like the meteorological range, be applied for photopical vision (cf. RUPPERSBERG, 1978). The radiance distributions and albedos — with absorption other than zero — over the entire solar spectral range can be calculated with the aid of the "Successive Orders of Scattering (SOS)" Program of QUENZEL (1979). It is thus possible in principle (although not planned for reasons of work capacity) to produce a SCOTRAN version SOS XX which applies in the solar spectral range to any wavelength outside the absorption range.

As in the earlier version (Ru), the interpolation functions IFSO in SCOTRAN version CIE 02 is equated to the regular transmittance between the extraterrestrial level z_e and z_m or z_o; the interpolation function IFSK for the relative radiance distributions in the upper hemisphere is equated to the regular transmittance between z_m and z, and those of the lower hemisphere to the regular transmittance between z_o and z (Ru, Section 5.2.2). An improved approximation function is used for IFAL (Section 3.2).

3.1   Rayleigh Sky in SCOTRAN Version CIE 02

In the case of the radiance distribution of a pure molecular atmosphere the airmass dependent on the viewing direction is taken into account, using the Sky Radiance Equation.

The following equation therefore replaces Ru, Equation (5.20):

$$_{ask}\Lambda_{Rayl}(\theta_{su}, \theta_{ski}, \Phi_{skj}) =$$

$$= \frac{3C}{16\pi} \frac{_{su}E_\lambda(z_e)}{} \frac{1 + \cos^2\gamma_{ij}}{1 - M(\theta_{su})/M(\theta_{ski})} (e^{-d_R(z_e, z_{ob}) M(\theta_{su})} - e^{-d_R(z_e, z_{ob}) M(\theta_{ski})}). \qquad (12)$$

(Caution: With $\theta_{su} = \theta_{ski}$ Equation (12) has the value 0/0. But the function is continous and differentiable, with a value given by the rule of de l'HOSPITAL. θ_{su} or $\theta_{ski} = 90°$ is also forbidden; Equation (14) allows max. approx. 89°).

The extraterrestrial irradiance at the 550 nm wavelength is $_{su}E_{\lambda = 550\ nm}(z_e) = 1.88\ Wm^{-2}\ nm^{-1}$ (NECKEL & LABS, 1984, Table X_a). In this paper we use the value $1.7250\ W^{-2}\ nm^{-1}$ reported by WOLFE and ZISSIS (1978, p. 3–35). Our results are not influenced evidently by this difference.

The angle γ_{ij} between the directions (θ_{su}, $\Phi_{su} = 0$) towards the sun and (θ_{ski}, Φ_{ski}) towards the area element of sky hemisphere in question is calculated from:

$$\cos\gamma_{ij} = \cos\theta_{su} \cos\theta_{ski} + \sin\theta_{su} \sin\theta_{ski} \cos\Phi_{skj}. \qquad (13)$$

For the airmass $M(\theta)$ (= $M(\theta_{su})$ or $M(\theta_{ski})$) $\simeq$ cosec θ for $\theta < 75°$ we use BEMPORAD's formula or NAGEL's improved approximation equation:

$$M(\theta_{su}) = \frac{1}{\sin(90° - \theta_{su} + 1{,}5(90° - \theta_{su})^{-0.72})}. \qquad (14)$$

For the sake of simplicity we shall use the Rayleigh sky which one would observe at a height of $z_{ob} = 3000$ m for all heights. This results in the optical thickness of the molecular atmosphere above this height:

$$d_R(z_e, z_{ob}) = 0.06267$$

and the scaling factors:

C =	66.58	67.44	68.54	70.37	75.57	79.94	92.69
for θ =	0°	30°	45°	60°	75°	80°	85°

3.2 The Interpolation Function IFAL in SCOTRAN Version CIE 02

The interpolation function IFAL is used to interpolate the albedo at level z between the reference levels z_m and z_0. This interpolation function controls the height dependence of the calculated slant visual range, e.g. when the target or observer enters a layer of fog. In SCOTRAN version CIE 01 IFAL was equated to the optical thickness between z_m and z as an experiment (Ru, Equation 5.30 f.). A comparison with OPAQUE test results in the meantime has indicated that this approximation is not a particularly good one; it was therefore improved in line with the following thinking.

Let us consider the layer of air between the levels z_m and z. For the incident radiation at the top let it have the reflectance $\rho(z_m, z)$, transmittance $\tau(z_m, z)$ and the absorptance $\alpha(z_m, z)$ and let us assume that the same values apply to the incident radiation underneath. This assumption is correct if the incident streams of radiation above and below have e.g. Lambertian angular distribution; the resultant form of IFAL is also regarded as adequate for the case of different angular distributions.

Beitr. Phys. Atmosph. Vol. 58, No. 1, February 1985

61

The albedo at level z is thus calculated as

$$A_L(z) = \frac{A(z_m) - \rho(z_m, z)}{\rho(z_m, z)\,(A(z_m) - \rho(z_m, z)) + (1 - \rho(z_m, z) - \alpha(z_m, z))^2} .$$ (15)

In general the following applies (even without the supposition made here):

$$\rho(z_m, z) = A_o(z_m, z).$$ (16)

$A_o(z_m, z)$ is the albedo which would be measured at level z_m if the layer of air at level z terminated in black, i.e. if the albedo there had the value zero. For the given direction of incidence of the sun radiation it is in accordance with PLASS and KATTAWAR (1968) or follows from the SOS program of QUENZEL (1979).

For this albedo we set for the case of Lambertian irradiation:

$$A_o(z_m, z) \rightarrow \overline{A}_o(d(z_m, z)).$$ (17)

This results from the values of PLASS and KATTAWAR by means of weighted integration (Ru, Equation (5.70)) over all directions of incidence. With a given particle distribution and given refractive index of the aerosol and cloud particles in the intermediate layer, this albedo is a clear function of the optical thickness of the layer of air under consideration. In the cases which are of interest here α can be disregarded with respect to ρ, and we obtain the following for the new interpolation function:

$$IFAL(z_m, z) \equiv A_L(z) = \frac{A(z_m) - \overline{A}_o(d(z_m, z))}{1 - \overline{A}_o(d(z_m, z))\,(2 - A(z_m))} .$$ (18)
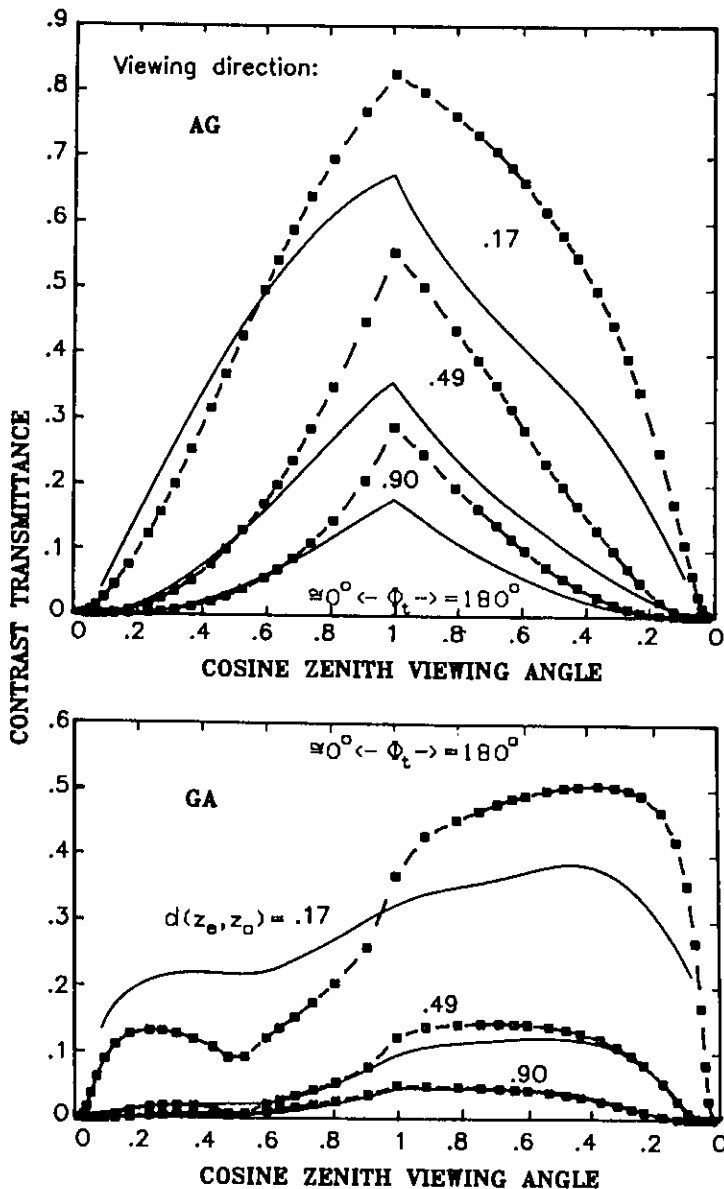
$A_L(z)$ cannot be used directly to represent the wanted variation in the albedo between reference levels z_m and z_o. If one of the suppositions is incorrect this $A_L(z)$ curve will end not at the given value $A(z_o)$ but at some smaller or larger value $A_L(z_o)$. The IFAL interpolation procedure (Ru, Section 5.3.3) causes a linear distortion of the $A_L(z)$ curve between z_m and z_o so that it passes through both given values $A(z_m)$ and $A(z_o)$.

4   Results

4.1   Comparison with the FASCAT Contrast Transmittance Model

Figure 3 shows a comparison with the results of the FASCAT contrast transmittance model developed in the USA by HERING (1981).

The contrast transmittance τ_c over the cosine of the viewing angle θ_t or the slant distance between the target and the observer is represented. The continuous lines mark the results of the HERING model, while the points enclosed in boxes are a selection of SCOTRAN calculations usually placed more closely together. The upper diagram in each case applies to the air-ground viewing direction (target on the ground which is assumed to be isotropic, ground albedo 0.1, observer at a height of 6 km), the lower diagram in each case to the ground-air viewing direction (target at a height of 6 km, observer on the ground). The left half of the diagrams applies to viewing directions up sun ($\Phi_t = 0°$), the right half to viewing directions with the sun behind ($\Phi_t = 180°$) — sun is at a zenith angle of $\theta_{su} = 60°$. In all cases a double-layered atmosphere with an inversion at a height of 3 km has been assumed. Above this height the (inversely proportional to the air density to level z = 0) reduced meteorological visual range $V_N(0)$ is in all cases 259 km, below it is $V_N(0) = 115$ (24.9; 12.4) km with the total optical thickness $d(z_e, z_o) = 0.17$ (0.49; 0.90). The single scattering albedo is 0.97 in the case of HERING, and 1.0 in our case.

Figure (top plot)

Viewing direction:

AG

.17

.49

.90

$\cong 0° \leftarrow \Phi_t \rightarrow = 180°$

CONTRAST TRANSMITTANCE

.9 .8 .7 .6 .5 .4 .3 .2 .1 0

0 .2 .4 .6 .8 1 .8 .6 .4 .2 0

COSINE ZENITH VIEWING ANGLE

Figure (bottom plot)

$\cong 0° \leftarrow \Phi_t \rightarrow = 180°$

GA

$d(z_e, z_o) = .17$

.49

.90

.6 .5 .4 .3 .2 .1 0

0 .2 .4 .6 .8 1 .8 .6 .4 .2 0

COSINE ZENITH VIEWING ANGLE

● **Figure 3**

Comparison between the HERING model and SCOTRAN.

Continuous lines: HERING calculation.

Points enclosed in boxes: Selection of SCOTRAN calculations.

Figure at the top: Target on the ground which is assumed to be isotropic (albedo 0.1), observer at a height of 6 km.

Figure at the bottom: Target at a height of 6 km, observer on the ground.

The three curves in each case apply to different optical thicknesses $d(z_e, z_o)$ of the overall atmosphere.

Above 3 km the (inversely proportional to the air density at level 0) reduced meteorological visual range is $V_N(0) = 259$ km in all cases.

Below it is $V_N(0) = 115$ km (24.9 km; 12.4 km), at $d(z_e, z_o) = 0.17$ (0.49; 0.90).

Some of the results for the two greater optical thicknesses coincide. In contrast to the HERING model, however, SCOTRAN shows a marked decrease in the contrast transmittance with viewing directions into the vicinity of the sun ($\theta_{su} \pm 5°$) and significantly larger contrast transmittances for air-ground viewing directions when viewing with the sun behind. SCOTRAN also reveals a large difference between some of the contrast transmittances in ground-air viewing directions when viewing up sun and with the sun behind.

In view of the large visual ranges in this comparison the portion of the path radiance, $_{su}L_\lambda^*$, generated by direct sun radiation is of great consequence; the form of the scattering function must therefore also show through clearly.
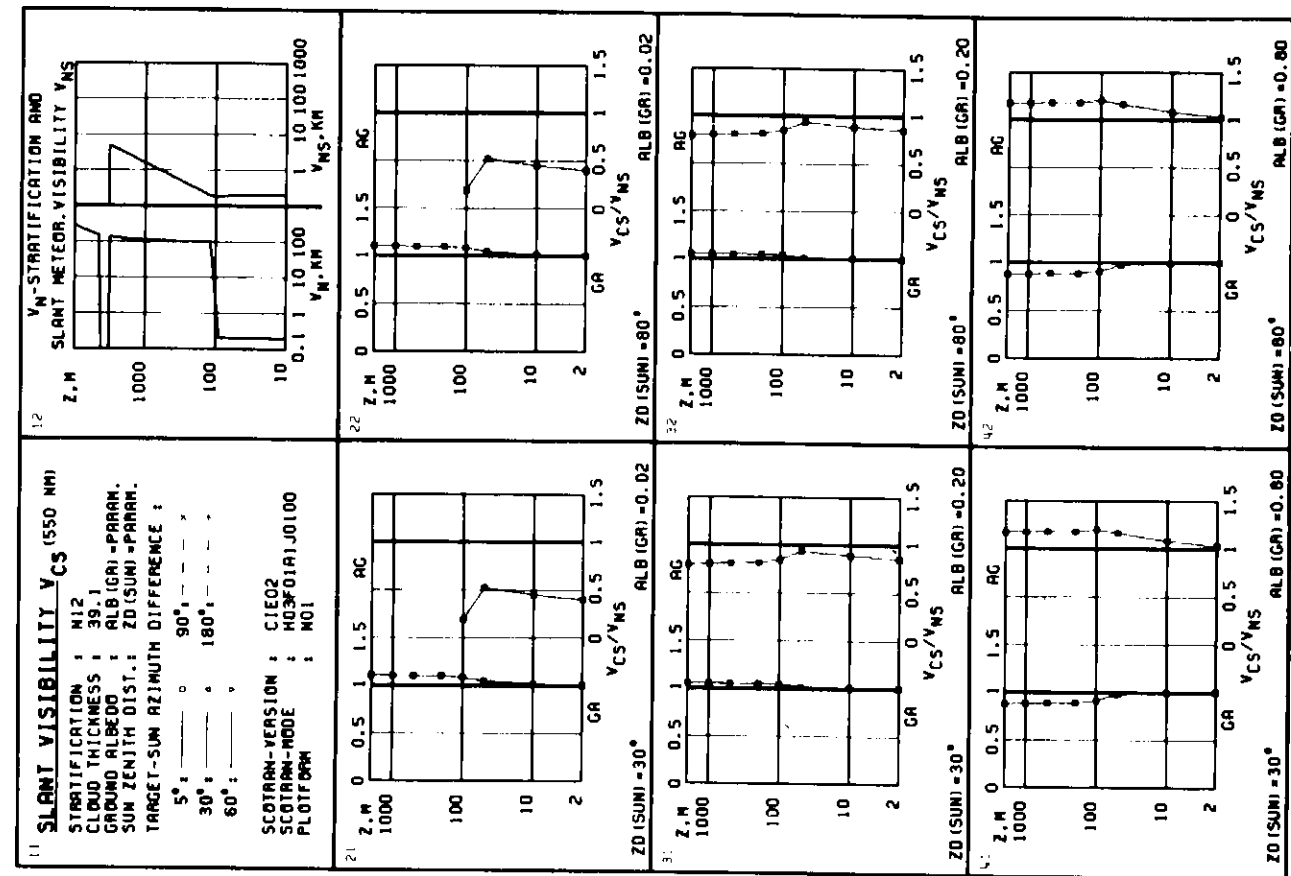
Figure 4 shows that using the HENYEY-GREENSTEIN scattering function (used by HERING) in $_{su}L_\lambda^*$ of SCOTRAN at large meteorological visual ranges actually results in a better approximation, but there is very little change in the smallest meteorological visual ranges (lowest curves) compared with Figure 3 which reveals clearly, as did v. REDWITZ et al. (1978), the small influence of the scattering function on the visual range in the case of greater turbidities.

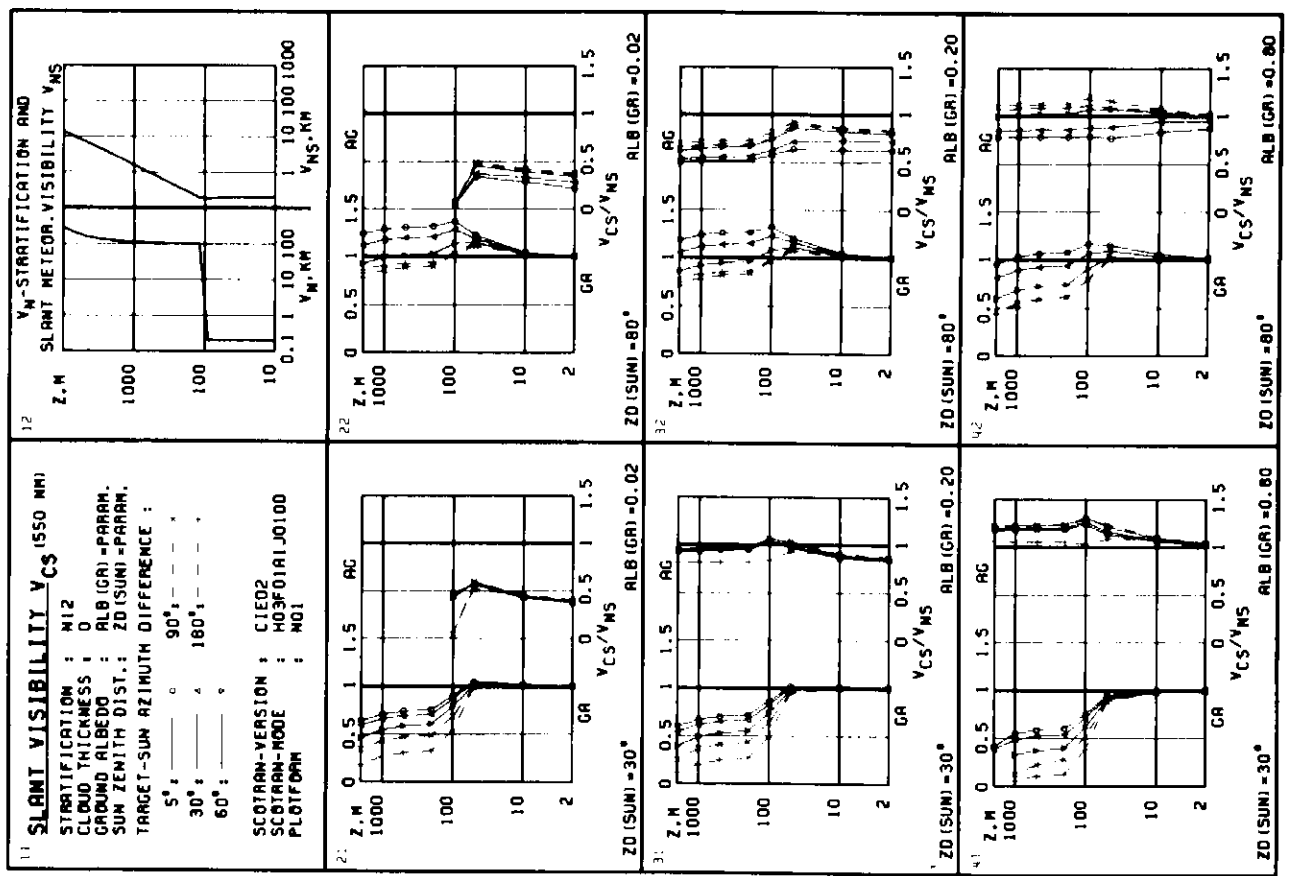Beitr. Phys. Atmosph. Vol. 58, No. 1, February 1985

63
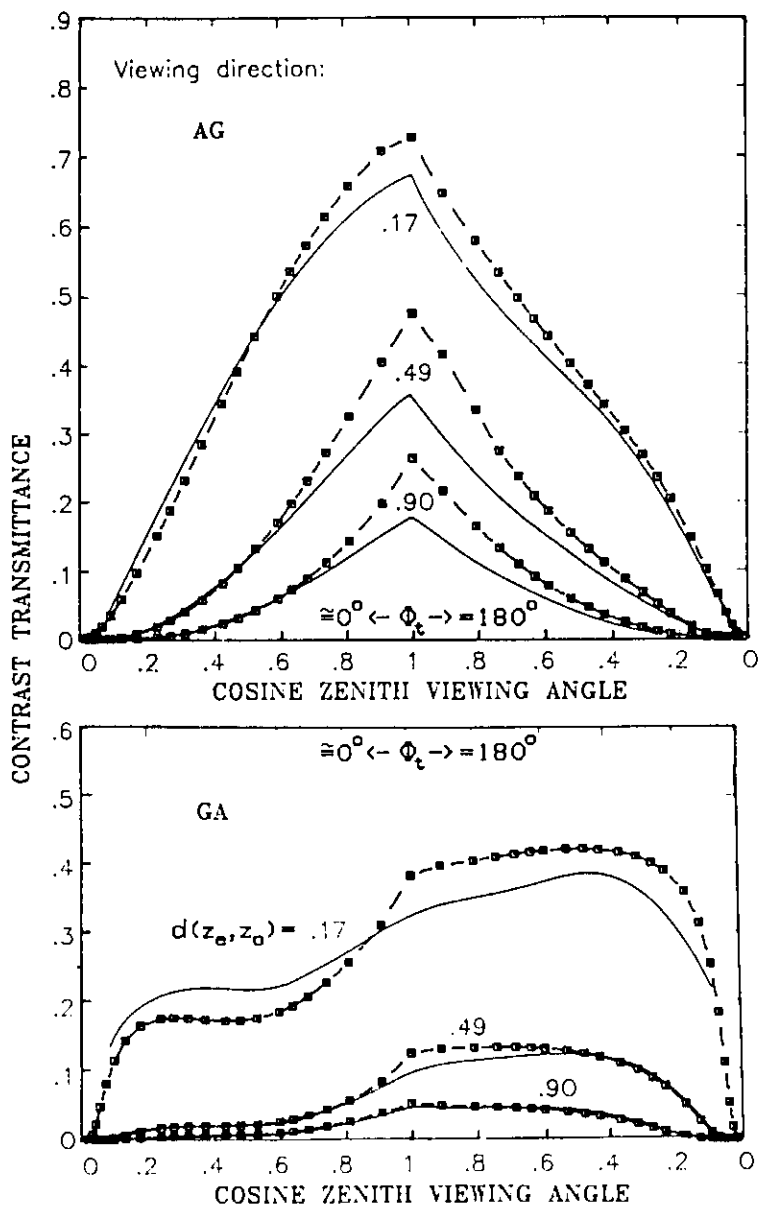
● Figure 4

Comparison between HERING model and modified SCOTRAN: As in the case of HERING the spectral path radiance generated by the primary sun radiation was also calculated in the SCOTRAN model using HENYEY-GREENSTEIN scattering functions.

Other comparative calculations have now been made for more turbid atmospheres, with stratifications approximately equivalent to those in Figures 5 and 6. With a clear sky and viewing directions into the solar azimuth the SCOTRAN transmittances are up to a factor of 2 below those of HERING (with the exception of major deviations in the direct vicinity of the sun ($\theta_{su} \pm 5°$)). The SCOTRAN slant visual ranges V_{CS} at these points are smaller than those of HERING by the factor 0.62. In all other cases the contrast transmittances of both models differ by less than 32 % and the slant visual ranges V_{CS} by less than 8 %.

It may be assumed that the correct values for the slant visual range lie somewhere between the values of the two models. The SCOTRAN version CIE 02 has a tendency to overemphasize the functional relationship between path radiance and azimuth because of its steep scattering functions for the direct scattered radiation. The opposite is probably true of the HERING model which ignores the functional relationship between the sky's radiance and the azimuth. There are of course slant visual ranges outside this gratifyingly narrow presumed error range which are due to effects which have not been dealt with here, e.g. anisotropy of the ground reflection. But they can be included easily as discussed at the end of Chapter 4 (Sky-Ground Ratio).

Figure 5 SCOTRAN results;

Figure 6 SCOTRAN results.

Boxes 11 and 12 give information on the parameter combinations and the way in which they are presented in the boxes below. Desription in the text.

Beitr. Phys. Atmosph. Vol. 58, No. 1, February 1985

65

4.2 SCOTRAN Slant Visual Ranges V_{CS}

We would like to obtain a general overview of the whole question of slant visual range. For this we use the SCOTRAN result tape which outputs the variation of the contrast transmittance τ_C with the distance between target and observer for a selection of observational and environmental parameters, and we compute the horizontal components of the distances for which $\tau_C = 2\%$. We call this quantity "2 %-contrast slant visual range" V_{CS}. V_{CS} is for practical purposes equal to the slant visual range of black (and not self-luminous) targets in daylight which subtend viewing angles of at least 20' (5.82 mrad).

V_{CS} like the slant meteorological visual range V_{NS} is a function of the meteorological visual range at ground level and its vertical course, but is also subject to the effects of irradiation of the atmosphere. This influence is made very clear in the quotient V_{CS}/V_{NS}. This quotient is therefore presented in the following Figures.

Each of the Figures 5–10 contains 8 "boxes": 11 (= line 1, column 1) to 42. Let us consider Figure 5 as an example:

Boxes 11 and 12 provide information on the parameter combinations and the way in which they are represented.

- V_{CS} (550 nm)
  This deals with the slant visual range V_{CS} (of large black targets in daylight) at 550 nm wavelength or the photopic spectral range.

- STRATIFICATION: N 12
  The turbidity stratification dealt with is No. 12 from one of the "Standard sequences" of 44 different turbidity stratifications selected by us. (It turned out to be advantageous to increase this number as against table 1 and to decrease the number of several other parameter variations; cf. RUPPERSBERG, BUELL and SCHELLHASE 1984).

  This turbidity stratification is shown in box 12 on the left as the variation of the horizontal meteorological visual range V_N with height z: Below a height of 90 m moderately dense fog prevails ($V_N(0) = 200$ m) and above a height of 120 m very good visibility with a reduced meteorological visual range $V_N(0) = 100$ km. It can be seen that the actual meteorological visual range V_N increases with height (inversely proportional to the air density).

  The resulting trend of the slant meteorological visual range is given on the right of box 12. Up to the ground inversion V_{NS} decreases to a value somewhat below 200 m and increases almost linearly above it.

- CLOUD THICKNESS: 0
  In this example the sky is cloudless. Figure 6 assumes clouds with an optical thickness of 39.1 — otherwise the turbidity stratification is the same — and this is shown in box 12. It is useful to note that a distance of the length of the meteorological visual range has an optical thickness of 3.91. In Figure 6 it could therefore be a 1 km thick stratus, for example, with a meteorological range of 100 m inside it. A situation such as this, however, in conjunction with radiation fog occurs at most during a short transition period.

- GROUND ALBEDO: ALB(GR) = PARAM. and

- SUN ZENITH DIST.: ZD(SUN) = PARAM.
  are fixed parameters in boxes 21–42.

- TARGET-SUN AZIMUTH DIFFERENCE
  Each of the following descriptions applies to three viewing direction azimuths towards the sun ($5°$; $30°$ and $60°$) and 2 laterally off the sun and with the sun behind ($90°$ and $180°$).

● SCOTRAN-VERSION: CIE 02
was discussed in Chapter 3.

● SCOTRAN-MODE
contains details of internal control parameters of the model (type of scattering functions, absorption case, "changeover level", at which a changeover is made from one scattering function to another) which can be varied within the version.

● PLOTFORM: N 01
In this plotform the parameter ZD(SUN) changes in the lower six boxes from left (30°) to right (80°) and the parameter ALB(GR) from top to bottom (0.02; 0.20; 0.80).

In each of the boxes 21 to 42 the quotient V_{CS}/V_{NS} is represented as a function of the height — left for ground-air viewing directions (GA; the observer is on the ground) and right for air-ground viewing directions (AG; the target is on the ground). The calculations were made for the heights z = (2; 10; 50; 100; 200; 500; 1000; 2000) m in each case. The calculated points are joined by straight lines so that the curve can be seen more easily. The lines sometimes stop at $V_{CS}/V_{NS} > 0$ — as in Figure 5, boxes 21 and 22, AG. In these cases the value 0 is reached before the next level up.

The quotient V_{CS}/V_{NS} for up to 67.680 parameter combinations is calculated in every figure of plotform N 01. The computing time on an IBM 3081 K is 107 seconds for the full number.

Now to the technical content of the diagrams.

Figure 5: When the sun is high (ZD(SUN) = 30°: left hand column) there is a wide spread of slant visual ranges V_{CS} from the ground (GA) to the large black target above the fog layer and each of them is considerably smaller than the slant meteorological visual range V_{NS}. For a target at a height of 2 km (see box 12) $V_{NS} \simeq 3.4$ km. With a ground albedo of 0.02 which is equivalent, for example, to a coniferous forest (KRIEBEL, 1978; KRINOV, 1953) this target can be detected at a distance (of its foot point from the observer) of $V_{CS} = 0.65 \times V_{NS} = 2.17$ km when viewed 5° close to the sun azimuth, and, surprisingly, less far with the sun behind: $V_{CS} = 0.17 \times V_{NS} = 580$ m. The detection ranges are somewhat smaller with a rocky or sandy background with the albedo 0.2 (cf. WOLFE and ZISSIS, 1978, p. 3–44; see also KRINOV, 1953), and with snow with an albedo 0.8 the detection range for this target in viewing directions away from the sun even approaches $V_{CS} = 0$.

An observer in the aircraft in question is at the same time totally incapable of perceiving a large black target on the ground (viewing direction AG) against a background of coniferous forest. Against a rocky or sandy background, however, he can detect it almost up to $V_{CS} = V_{NS} = 3.4$ km, and over snow even somewhat further. If on the other hand the target is in a snow-covered clearing (albedo in the clearing: 0,8, above the wood: 0,02; radiance ratio in equation (8): k = 0.8/0.02 = 40) the contrast transmittance at distances V_{CS}, which are entered in Figures 5 and 6, is not 0.02, but according to Equation (9) 0.45. The target is therefore clearly visible against this background and its slant visual ranges $V_{CS}^{(lb)}$ and quotients $V_{CS}^{(lb)}/V_{NS}$ are considerably larger than the values in Figures 5 and 6 (boxes 21 and 22). When the sun is low (ZD(SUN) = 80°: righthand column) there is a wider spread of AG slant visual ranges to the ground with larger ground albedos, and one sees considerably further with the sun behind than up sun. The conditions in this viewing direction (AG) correspond precisely to common experience, when the sun is high or low. With upward viewing directions (GA), however, all slant visual ranges shift — again surprisingly — to larger values and the spread remains wide with large slant visual ranges towards the sun.

This is contrary to expectations but not as far as we know to experience, since we do not know of any: Systematic observations in this respect are disproportionately more difficult than AG observations, and chance observations in this direction would probably be ascribed to atmospheric inhomogeneities etc. because of one's preconceived expectations.

How can one understand these two unexpected effects, or the third one either which can be seen from Figure 6, whereby the slant visual range GA decreases so rapidly when the sun is high (not, however, when it is low) when the target is flying above the upper boundary of the fog. It is easy to find a plausible explanation:

With very good visibility ($V_N(0) = 100$ km), the sky (at 550 nm) above the fog layer appears very dark when the sun is high — and in the region away from the sun considerably darker than in the region close to the sun. A black target therefore does not stand out very well and in the region away from the sun even less well than in the region close to the sun. This effect is apparently more noticeable with GA visibility than the path radiance at the location of the observer which is greater in the region near the sun and hence causes greater disturbance. This can be explained somewhat less graphically using Equation (6): the spectral inherent radiance $_bL_{\lambda_0}$ of the background is smaller in the region away from the sun than close to the sun, while the spectral path radiance L_λ^* viewed from the base of the fog layer differs only slightly with the azimuth. The contrast transmittance τ_C in viewing directions towards the sun is therefore greater than with the sun behind. When the sun is low the sky is brighter overall — relative to the vertical radiant flux density of the direct sun radiation — and the GA slant visual ranges increase.

Figure 6 shows the effect of a cloud layer with optical thickness 39.1 (completely covering the direct sun radiation) — otherwise the turbidity stratification is unchanged.

In line with the preceding explanation the three unexpected effects which were apparent in Figure 5 disappear. The slant visual range GA is $V_{CS} \simeq V_{NS}$ in all cases. From a location above the fog layer it is absolutely impossible to perceive black targets on the ground against a background of coniferous forest (ALB(GR) = 0.02); against a rocky or sandy background (ALB(GR) = 0.2) they can be perceived somewhat less far than V_{NS} and over snow (ALB(GR) = 0.80) even somewhat further. This is surprising but easily understood in the context of the sky-ground ratio discussed further on. Otherwise the contents of Figure 6 do not conflict with practical experience or with expectations.

Figure 7 shows a similar turbidity stratification to Figure 5 except that below a height of 90 m there is only light fog with a reduced meteorological visual range $V_N(0) = 500$ m.

Apart from the fact that at the low ground albedo of 0.02 the AG slant visual ranges are only about half as large as the GA slant visual ranges it is conspicious that the spread of the GA slant visual ranges is by no means as wide as in Figure 5. For the explanation of the three unexpected effects in Figure 5 to be consistent we must assume that the variation of path radiance as a function of the azimuth, which offsets the effect, at the location of the observer is considerably greater in Figure 7 than in Figure 5. That is the case for in Figure 5 (box 21) the direct sun radiation is only transmitted to the observer on the ground with a transmittance of 0.056 and somewhat more, but in Figure 7 with a transmittance of 0.26.

Figure 8 confirms this explanation. In contrast to the preceding figures, the inversion height Z(INV) is parameter and the results are shown here in PLOTFORM N04: box 21 contains the results of the same box in Figure 7, and the inversion height increases from box to box.

We see that with increasing inversion height, up to Z(INV) = 270 m, the spread actually reaches the extent and the sign observed in Figure 5! In box 32 the curves stop at z = 200 m. As already mentioned this means that the value $V_{CS} = 0$ is reached before the next measurement point (500 m) for all viewing direction azimuths. The sharp increase in the quotient V_{CS}/V_{NS} in boxes 41 and 42 in viewing direction GA and with an target height of 500 m does not mean much in practice, for V_{NS} (and hence also V_{CS}) is almost equal to zero at this height.
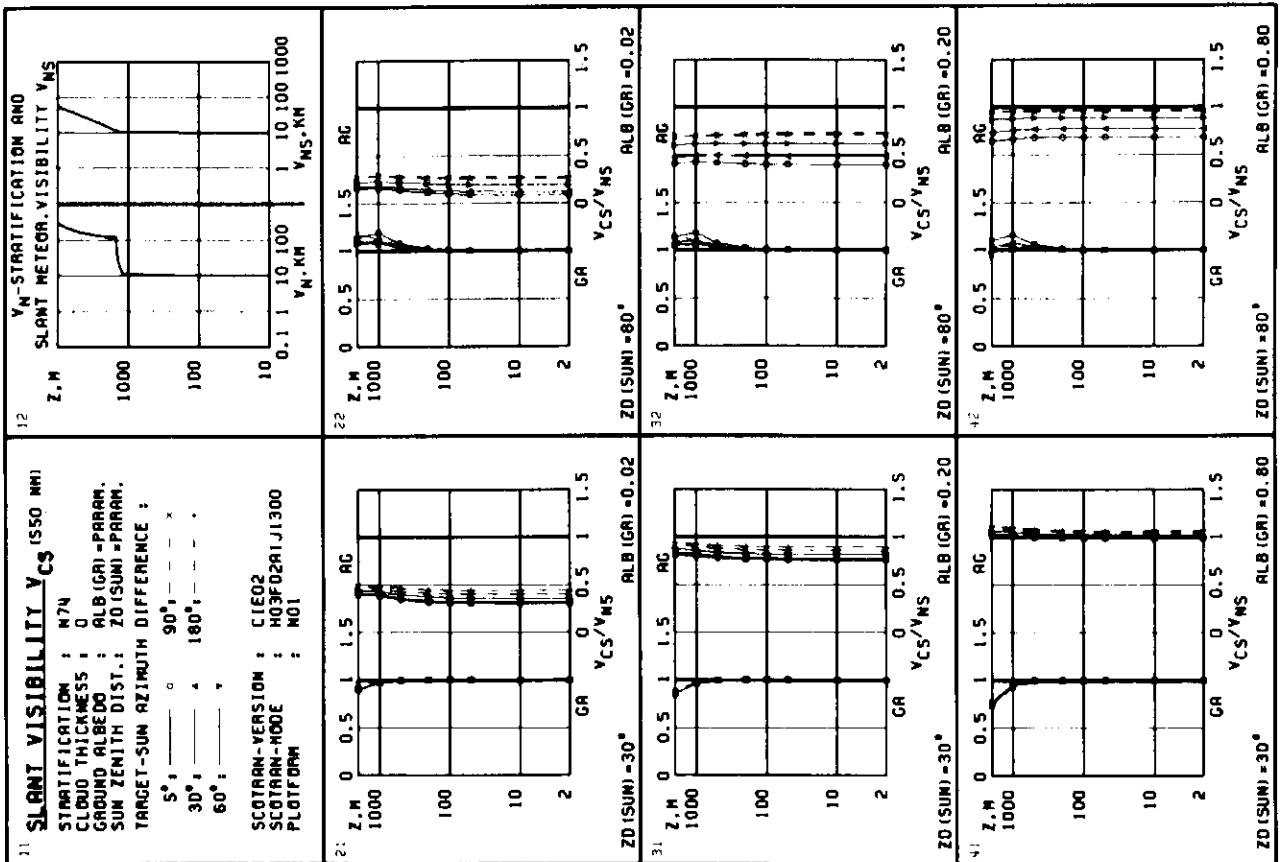
Figure 9 shows the situation with light haze ($V_N(0) = 10$ km) under a boundary layer inversion at a height of 1200 m — 1500 m and very good visibility ($V_N(0) = 100$ km) above it. With viewing directions towards the ground (AG) it is possible to see further with the sun behind, and even much further when the sun is low, than when looking up sun. This is confirmed by practical experience. The slant visual range V_{CS} upwards (GA) is, however, not a function of the azimuth up to a target height of a few
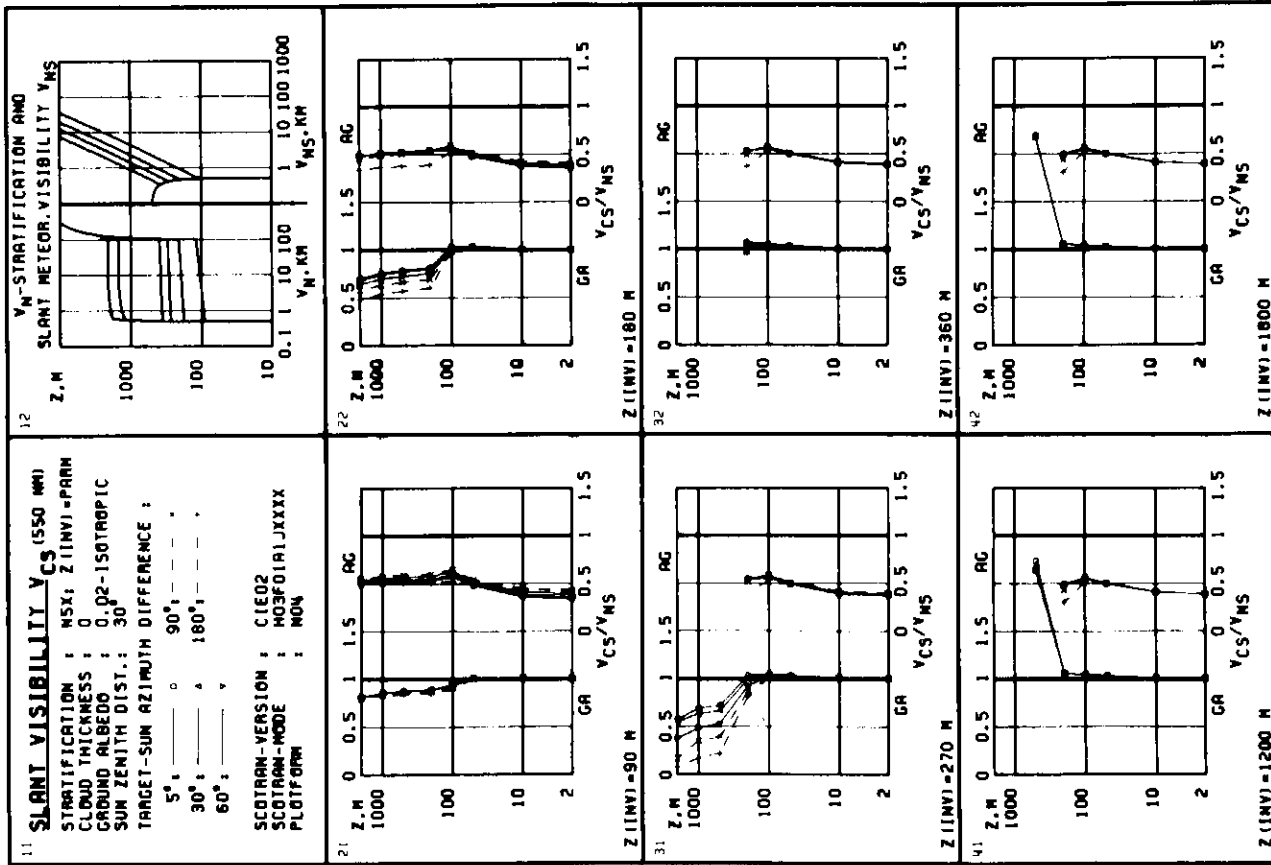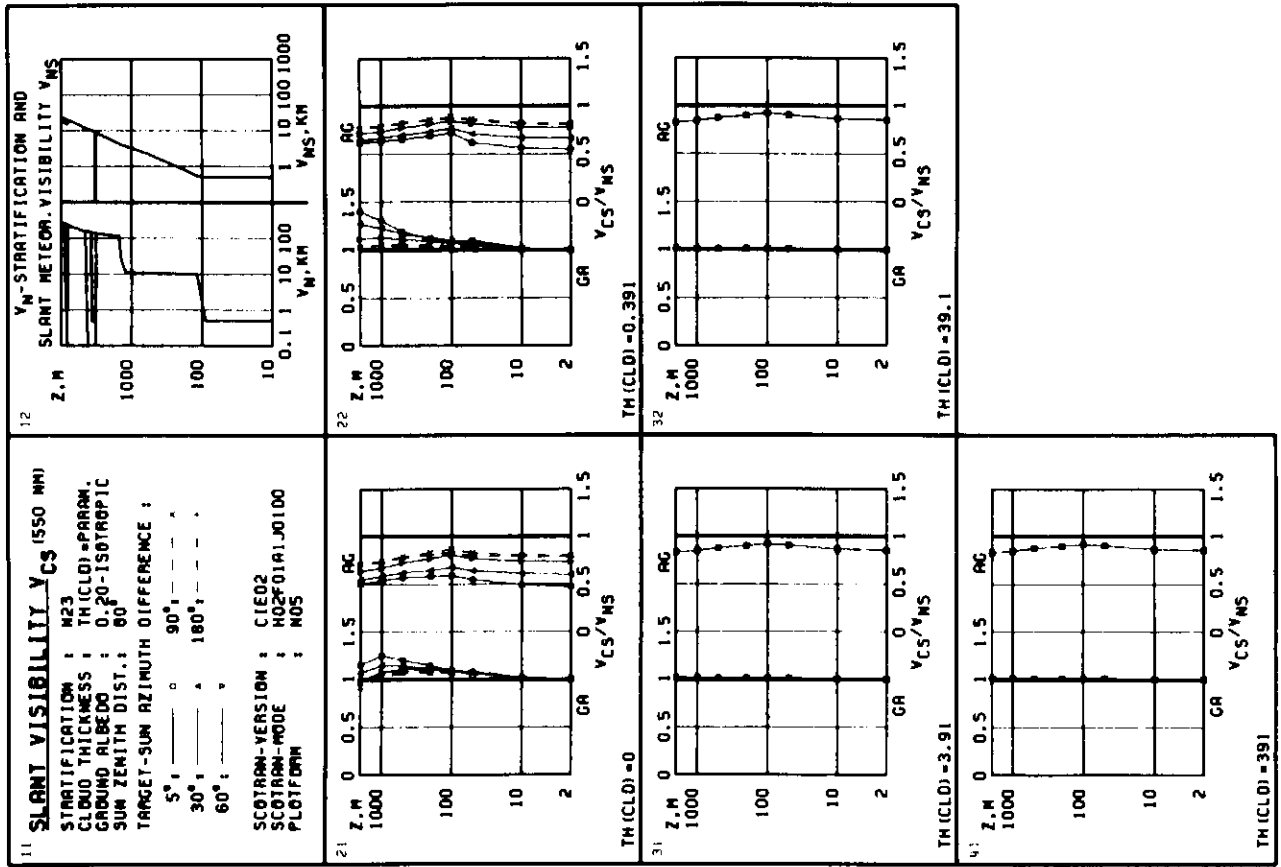
● Figure 8 SCOTRAN results.
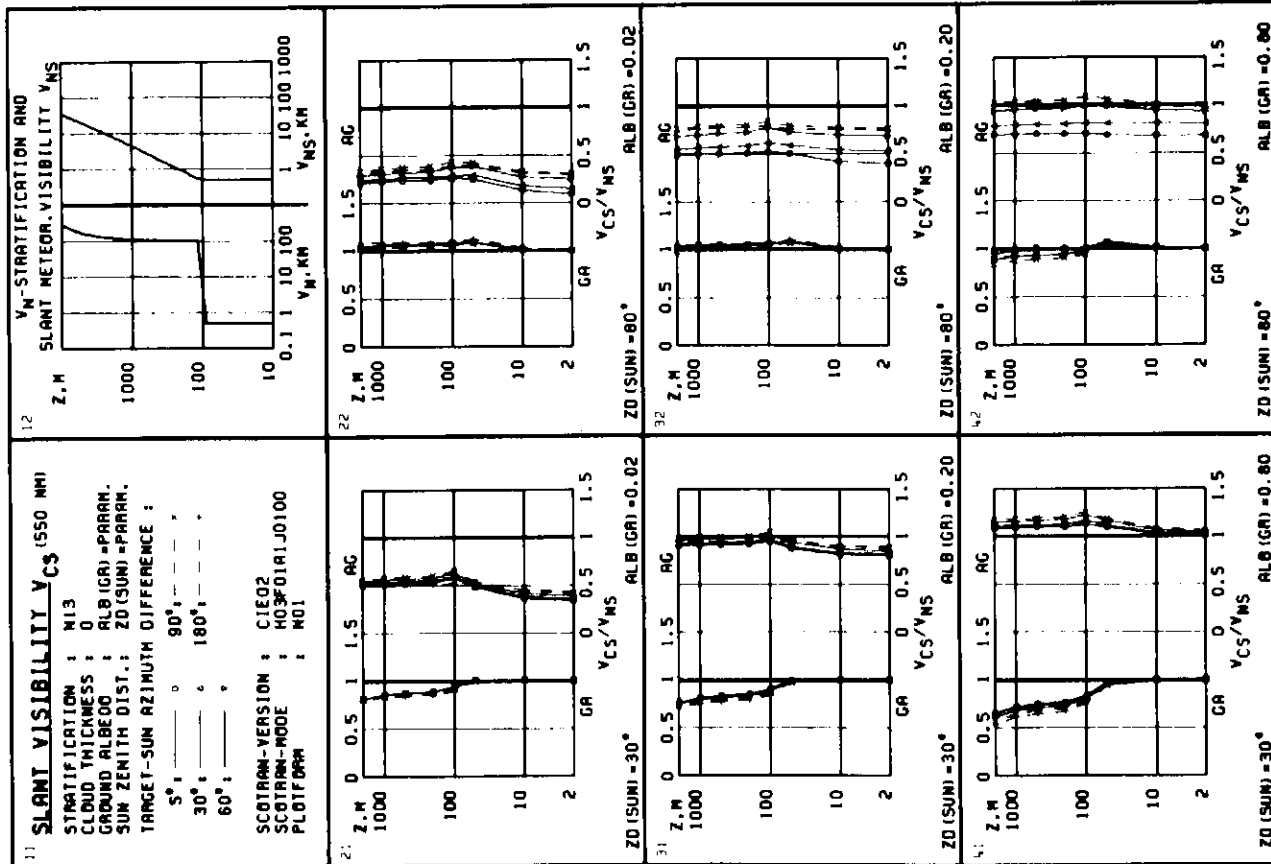
● Figure 7 SCOTRAN results.

Figure 10 SCOTRAN results.

Figure 9 SCOTRAN results.

hundred metres which is surprising at first. This result is in fact correct and shows the target heights up to which the horizontal meteorological visual range V_N can in practice be taken for the slant visual range V_{CS}. The invariance of V_N as a function of the azimuth was also a surprising result of KOSCH-MIEDERs theory which was strongly doubted at first but was soon shown to be correct experimentally.

Finally Figure 10 shows the effect of cloudiness, but otherwise with the same turbidity as in Figure 8. A cloud layer with the optical thickness 0.391 (e.g. a thin stratus) has a noticeable effect on the slant visual ranges in the boundary layer (box 22). There is no longer any noticeable functional dependence of the slant visual range on the azimuth in the case of the optically thicker cloud cover (3.91) of box 31, through which the sun can still be detected clearly, and greater optical thicknesses of cloud (boxes 32 and 41) do not alter slant visual range conditions further. This is also so with ground fog (Figure 6) and according to the results of SCOTRAN version CIE 02, this appears to be so generally.

The sky-ground ratio SGR which is the quotient from the luminance of the horizon sky near the target and the inherent luminance of the target background plays a great role in the visual range of targets near the horizon against a terrestrial background (e.g. the edge of a wood). Equation (9) for the special case of horizontal viewing direction ($\tau_C = \tau_r$ and $1/k$ = SGR) equals the SGR-equation of DUNTLEY (1948) and SIEDENTOPF (1948). The SGR can be calculated easily from the lowest V_{CS}/V_{NS} values for the viewing direction AG in each of Figures 5–10 (cf. RUPPERSBERG, BUELL and SCHELLHASE, 1984):

$$\frac{1}{3.912} \ln \left(\frac{49}{SGR(z)} + 1 \right) \cong \frac{V_{CS}}{V_{NS}} . \tag{19}$$

As far as the SGR turns out to be constant with height it is applicable on slant visibility problems too in its meaning mentioned above using the mentioned special form of Equation (9).

MIDDLETON (1952, Table 4.1) and HOFFMANN (1979) on the other hand give a number of measured SGRs. Comparable SCOTRAN values are set side by side in Table 2. The stratification figures from Figure 9 without and with cloudiness were used by SCOTRAN.

It can be seen that the comparable results are largely the same while the results of the different examples 1, 2, 3 differ significantly from one another. SCOTRAN, however, shows a tendency towards large SGRs which is doubtless connected with the isotropy of the ground reflection which is assumed in these examples.

The natural surface of the earth almost always appears brighter towards the horizon than with steeper viewing directions downwards (KRIEBEL, 1978; KRINOV, 1953; WOLFE & ZISSIS, 1978). This is due to

■ Table 2 Comparison between SCOTRAN sky-ground ratios and measured values reported by MIDDLETON (1952, Table 4.1) and HOFFMANN (1979)

Case No.	MIDDLETON		HOFFMANN		SCOTRAN – Version CIE 02				
	sky/ground cond.	SGR	illumination/background	SGR	STRAT;	TH(CLD);	ZD(SUN);	ALB(GR)	SGR
1	overcast/forest	25	sunlit ⎫ forest edge	6–22	No. 74 ;	0 ;	80 ;	0.02	128–26
	clear/forest	5	shade ⎬ +	6–7	No. 74 ;	0 ;	30 ;	0.02	22–11
			half-shadow ⎭ green grass	5–8	No. 74 ;	39 ;	80–30 ;	0.02	18
2	overcast/desert	7	shade/green corn	3–5	No. 74 ;	0 ;	80 ;	0.20	3–3.0
	clear/desert	1.4	shade/yellow sandy	1–2	No. 74 ;	0 ;	30 ;	0.20	2.7–1.5
			soil		No. 74 ;	39 ;	80–30 ;	0.20	2.3
3	overc./fresh snow	1			No. 74 ;	0 ;	80 ;	0.80	3.7–1.1
	clear/fresh snow	0.2			No. 74 ;	0 ;	30 ;	0.80	1.1–0.8
					No. 74 ;	39 ;	80–30 ;	0.80	1.0
					No. 12 ; ⎫	0 ;	30 ;	0.80	0.8–0.3
					z = 100 m ⎭	39 ;	30 ;	0.80	0.4

its reflection anisotropy and not only to brightening by the path radiance. The inherent radiances of target backgrounds near the horizon are therefore greater and the SGRs consequently smaller than they would be with isotropic ground reflection. The fog surfaces at a height of $z = 100$ m in the examples of Figures 5 and 6 reflect anisotropically and in fact they show SGRs between 0.3 and 0.8 with ground albedos of 0.8 - approximately the figures given by MIDDLETON for snow (see Table 2).

SCOTRAN can make allowance for anisotropy of the ground reflection. A resultant halving of the SGRs would have a less marked effect on the V_{CS}/V_{NS} values: this would produce quotients 12 % (17 %; 32 %; 55 %) greater at $V_{CS}/V_{NS} = 1.5$ (1.0; 0.5; 0.2) for viewing directions downwards (AG) rather than the values shown in Figures 5–10. There is far less change in the values for upward viewing directions (GA).

5 Conclusion

When applied to a selection of observational and environmental parameters, SCOTRAN gives results which give a clear picture of the interaction of these parameters with the phenomenon of slant visual range. This picture is partly in line with experiences, but partly also shows effects which one would not have assumed, but can be explained logically and also readily understood once they have been drawn to attention. In wide ranges which can be detected and delimited by SCOTRAN the complicated slant visual range V_{CS} (of large black targets in daylight) almost agrees with the mathematically and physically very simple slant meteorological visual range V_{NS}, or can be determined from it with the aid of the sky-ground ratio. The slant visual range of targets which are not large and black, even at dusk and at night, follows from SCOTRAN or V_{NS} in conjunction with the target parameters and the known thresholds of contrast.

In terms of quantity the results differ in a number of comparative calculations — excluding viewing directions up sun — from those of the FASCAT model developed by HERING by less than 32 % in the contrast transmittances and by less than 8 % in the slant visual ranges V_{CS}. SCOTRAN sky-ground ratios agree satisfactorily with measured values; the influence of the reflection anisotropy of the ground is not taken into account here but can easily be estimated.

All in all SCOTRAN supplies a clear and realistic overview of the effects on the slant visual range of the different observational and environmental parameters and of some target parameters as well.

References

BAKKER, T., 1975: The measurement program OPAQUE of AC/243 (Panel IV/RSG 8) on "sky and terrain radiation", AGARD-CP No. 183, p. 14. 1–10.

BUELL, R. H., 1984: The DFVLR Contrast Transmittance Model SCOTRAN-Programme System: Description and Operating Instruction. DFVLR- FB 84–18.

CIE, 1970): International Lighting Vocabulary, 3 rd edition common to the CIE and IEC. International Commission on Illumination, Bureau Central de la CIE. 4Av. Recteur Poincaré, 75 Paris 16, France.

DIN 5037, Bl. 2, 1963: Normenblatt Lichttechnische Bewertung von Scheinwerfern.

DUNTLEY, S. Q., 1948: The reduction of apparent contrast by the atmosphere. JOSA 38, 179–190.

DUNTLEY, S. Q., 1948: The visibility of distant objects. JOSA 38, 237–247.

DUNTLEY, S. Q., BOILEAU, A. R. and PREISENDORFER, R. W., 1957: Image transmission by the troposphere I. JOSA 47, 499- 506.

DUNTLEY, S. Q., JOHNSON, R. W. and GORDON, J. I., 1964: Ground-based measurements of earth-to-space beam transmittance, path radiance, and contrast transmittance. University of California, San Diego, Scripps Institution of Oceanography, Visibility Laboratory, Tech. Doc. Rept. No. Al-TOR-64-245.

DUNTLEY, S. Q., JOHNSON, R. W. and GORDON, J. I., 1978: Airborne measurements of atmospheric volume scattering coefficients in northern europe, fall 1976. AFGL-TR-77-0239. Prepared for Air Force Geophysics Laboratory, Air Force Systems Command, USAF, Bedford, Massachusetts 01731 SIO Ref. 78–3.

GORDON, J. I., 1978: Airborne measurements of optical atmospheric properties. Summary and review III. AFGL-TR-78-0286, SIO Ref. 79–5.

FENN, R. W., 1978: OPAQUE-A measurement program of optical atmospheric quantities in Europe. Volume I-The NATO OPAQUE Program. AFGL-TR-78-0011, Spec. Rep. No. 211. Optical Physics Division Air Force Geophysics Laboratory, Air Force Systems Command, USAF, Hanscom AFB, Massachusetts 01731.

FOITZIK, L., 1947: Theorie der Schrägsicht. Z. f. Meteorologie 6, 161–175.

HERING, W. S., 1981: An operational technique for estimating visible spectrum contrast transmittance. AFGL-TR-81-0198; SIO 82–1.

HOEHN, D. H., 1981: Einleitung zum Lehrgang P 1.03, 1981: Sicht und Sichtmessung unter besonderer Berücksichtigung des IR-Bereiches. Manuskript Nr. 1, Seite 7. CCG, D-8031 Oberpfaffenhofen.

HOFFMANN, H.-E., 1983: Physiologisch-optische Effekte und Wahrnehmungskriterien. DFVLR-IB 553-83-14.

HOFFMANN, H.-E., BUELL, R. H. and KUEHNEMANN, W., 1979: Summaries of some reports of 1978 concerning results of field experiments for visibility. DFVLR-Mitt. 79-11.

JOHNSON, R. W. and GORDON, J. I., 1982: A review of optical data analysis related to the modelling of visible and optical infrared atmospheric properties. AFGL-TR-82-0086; SIO 83-5.

KASTEN, F., 1962: Sichtweite und Albedo, insbesondere im Polargebiet. I. Theorie der horizontalen Sichtweite nicht selbstleuchtender Objekte unter bedecktem Himmel. Beitr. Phys. Atmosph. 34, 234–258.

KASTEN, F. and RASCHKE, E. 1972: Nomenklatur zur Beschreibung von Strahlungsmessungen und -Rechnungen. BMBW-FB W 72-20.

KOSCHMIEDER, H., 1925: Theorie der horizontalen Sichtweite. Beitr. Phys. fr. Atmosph. 12, 33–55 and 171–181.

KRIEBEL, K. T., 1978: Measured spectral bidirectional reflection properties of four vegetated surfaces. Applied Optics 17, 253–259.

KRINOV, E. L., 1953: Spectral reflectance properties of natural formations. Aero Methods Laboratory, Academy of Sciences, U.S.S.R. Translation: NRC TT-439, National Resarch Council of Canada.

MIDDLETON, W. E. K., 1952: Vision through the atmosphere. University of Toronto Press.

NECKEL, H. and LABS, D., 1984: The solar radiation between 3300 and 12500 A. Solar Physics 90, 205–258.

OVERINGTON, J., 1976: Vision and acquisition. London: Pentech Press; New York: Creme, Russack & Co., Inc.

PLASS, G. N. and KATTAWAR, G. W., 1968: Monte Carlo calculations of light scattering from clouds. Appl. Optics 7, 415–419.

QUENZEL, H., 1979: Berechnungen der Strahldichteverteilung des Himmels mit Hilfe eines Successive Orders of Scattering-(SOS-) Programms. Private communication: Meteorologisches Institut der Universität München (MIM), Theresienstr. 37, D-8000 München.

RASCHKE, E. (ed.), 1978: Terminology and units of radiation quantities and measurements. International Association of Meteorology and Atmospheric Physics (IAMAP), Radiation Commission. NCAR, Boulder, Colorado, U.S.A.

v. REDWITZ, H., RUPPERSBERG, G. H., SCHELLHASE, R. and WEIDNER, J., 1978: Interpretation of airborne measurements of atmospheric extinction and irradiating fluxes in Germany and The Netherlands. AGARD-CPP-238, p. 37.1–12.

RUPPERSBERG, G. H., 1978: The correct spectral weighting of the meteorological visibility. Beitr. Phys. Atmosph. 51, 247–256.

RUPPERSBERG, G. H., 1979: Ein numerisches Modell für die Schrägsichtweite – Grundlagen – DFVLR-IB 553-5-79.

RUPPERSBERG, G. H., 1982: Grundlagen für ein numerisches Modell der Schrägsichtweite. DFVLR-FB 82-01.

RUPPERSBERG, G. H., BUELL, R. H. and SCHELLHASE, R., 1984: Die Schrägsichtweite. To be published as BMVg-FBWT.

RUPPERSBERG, G. H. and SCHELLHASE, R., 1979: Slant meteorological visibility. Optica Acta 26, 699–709.

SIEDENTOPF, H., 1948: Über Dämmerungssicht, Detailsicht und Flugsicht. Zeitschrift für Meteorologie 2, 110–115.

WEISS, I., 1976: Die Möglichkeit der Vorhersage der Schrägsicht beim Landeanflug mit Hilfe routinemäßig anfallender Wetterbeobachtungen nach einer niederländischen Studie, Flugsicherheit 3, 4–6.

WOLFE, W. L. and ZISSIS, G. J. (eds.), 1978: The Infrared Handbook. Prepared by The IRIA Center, Env. Res. Inst. of Michigan for the Off. of Nav. Res., Dept. of the Navy, Wash., DC.